Supporting Information

Hybrid of g-C_3N_4 Assisted Metal−Organic Frameworks and Their Derived High-Efficiency Oxygen Reduction Electrocatalyst in the Whole pH Range

Wenling Gu,[Ɨ§] Liuyong Hu,[£§] Jing Li[*Ɨ] and Erkang Wang[*Ɨ]

[Ɨ]State Key Laboratory of Electroanalytical Chemistry, Changchun Institute of Applied Chemistry, Chinese Academy of Sciences, Changchun, Jilin 130022, PR China;

[£]State Key Laboratory of Polymer Physics and Chemistry, Changchun Institute of Applied Chemistry, Chinese Academy of Sciences, Changchun, Jilin 130022, PR China;

[§]University of the Chinese Academy of Sciences, Beijing, 100049, PR China

Corresponding author: Associate Prof. Jing Li, Prof. Erkang Wang, Tel: +86-431-85262003, Email: lijingce@ciac.ac.cn and ekwang@ciac.ac.cn

Detailed Experimental Section

Chemicals and Reagents

Iron trichloride hexahydrate ($FeCl_3 \cdot 6H_2O$), urea, sulphuric acid (H_2SO_4), potassium hydroxide (KOH), anhydrous ethanol and dimethylformamide (DMF) were obtained from Beijing Chemical Reagent (Beijing, China). 2-Aminoterephthalate, 5% Nafion and 20% E-TEK Pt/C were purchased from Alfar Aesar (Tianjin, China). The aqueous solutions of 0.1 M KOH, 0.1 M PBS (pH = 7.4) and 0.5 M H_2SO_4 were prepared by Millipore Mill-Q (18.2 MΩ cm) deionized water.

Apparatus

Powder X-ray diffraction (XRD) was measured with a D8 ADVANCE (Germany) using Cu Ka radiation (λ =1.5406 Å). Transmission electron microscopy (TEM), high-resolution transmission electron microscopy images (HRTEM), high angle annular dark field-scanning transmission electron microscopy (HAADF-STEM) and elemental mapping images were carried out on a TECNAI G2 high-resolution transmission electron microscope (Hitachi, Tokyo, Japan). X-ray photoelectron spectroscopy (XPS) was obtained an ESCALAB-MKII X-ray photoelectron spectroscopy (VG Scientific, UK). Scanning electron microscope (SEM) and Energy dispersive X-ray (EDX) spectras were carried out on an XL30 ESEM FEG SEM (Philips, Netherlands). The nitrogen adsorption/desorption isotherms were recorded by a Quantachrome Adsorption Instrument. Thermogravimetric analysis (TGA) was measured with NETZSCH STA 449F3. Linear sweep voltammetry (LSV), Cyclic voltammetric (CV) and amperometric i-t curves were measured on a CH Instruments

832 voltammetric analyzer (Shanghai, China). Rotating ring-disk electrode (RRDE) and rotating disk electrode (RDE) techniques were tested on a Pine electrochemical instrument (Co. Ltd. USA). The electrochemical measurements were all recorded on a CHI 832C electrochemical station with an Ag/AgCl (saturated KCl) electrode and a platinum wire as the reference electrode and counter electrode, respectively, while the RRDE electrode modified catalyst ink as the working electrode.

In this work, the potentials were all converted to the reversible hydrogen electrode (RHE) according to E (*vs*. RHE) = E (*vs*. Ag/AgCl) +0.197 + 0.059 pH.

The transferred electron number (n) and % H_2O_2 (the percentage of H_2O_2 released during ORR) were calculated with the equation of

$$n = \frac{4i_d}{i_d + i_r / N}$$

$$H_2O_2\% = \frac{200 i_r / N}{i_d + i_r / N}$$

Here, the i_d is the current obtained from disk electrode, i_r stands for current from ring electrode and N is the collection efficiency of 0.37.

The RDE measurements were performed in an O_2-saturated 0.1 M KOH, 0.5 M H_2SO_4 or 0.1 M PBS electrolyte by a negative-direction sweeping potential with different electrode rotation rates. The transferred electron number also can be calculated according to the Koutecky–Levich equations:

$$\frac{1}{j} = \frac{1}{j_k} + \frac{1}{B\omega^{0.5}}$$

$$B = 0.2nF(D_0)^{2/3} v^{-1/6} C_0$$

where j is the current density, j_k represents the kinetic-limiting current density, ω is the electrode rotation rates, n is the transferred electron number, F is the Faraday constant, D_0 is the diffusion coefficient of O_2, v is the kinematic viscosity of the electrolyte, C_0 is the bulk concentration of O_2.

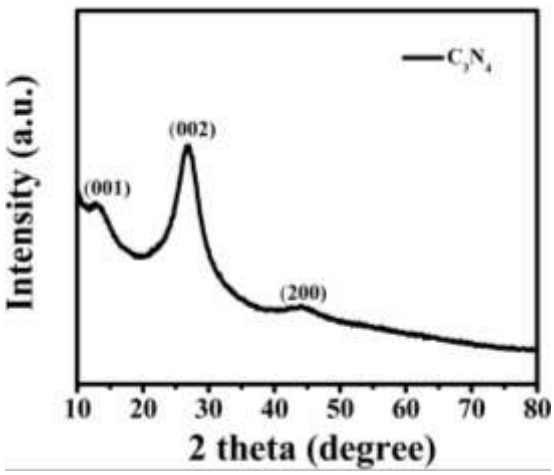

Figure S1 XRD pattern of g-C_3N_4.

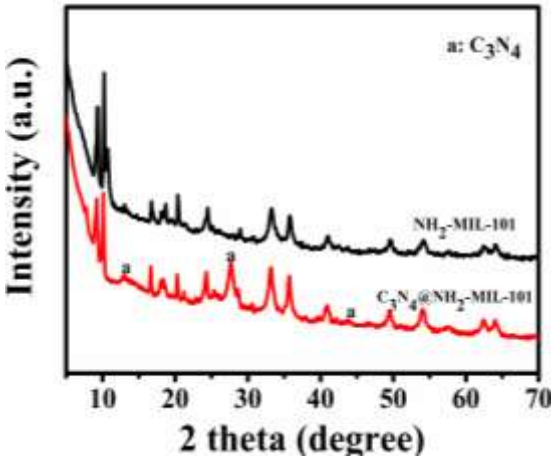

Figure S2 XRD patterns of NH_2-MIL-101 and C_3N_4@NH_2-MIL-101.

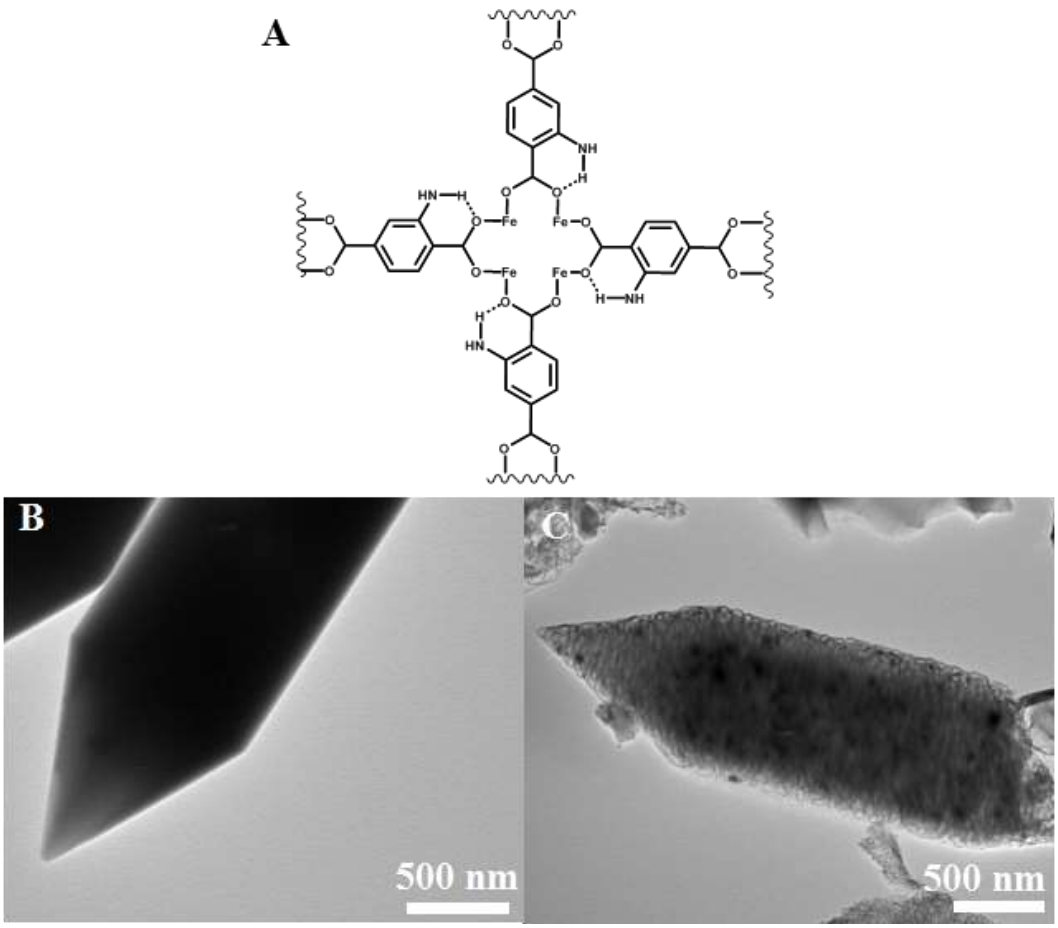

Figure S3 The structure introduction of NH_2-MIL-101 (A); TEM images of NH_2-MIL-101 (B) and NH_2-MIL-101-700 (C).

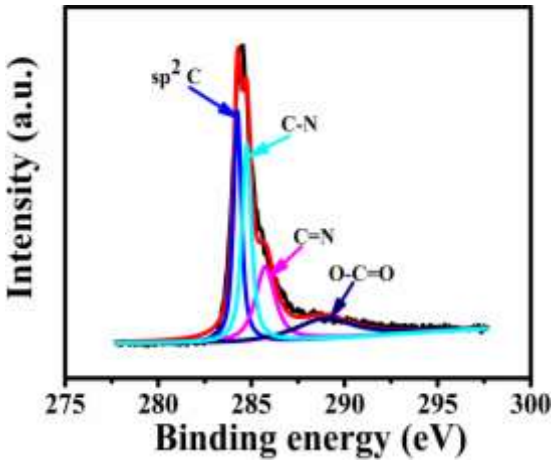

Figure S4 High resolution C 1s spectra of the obtained C_3N_4@NH_2-MIL-101-700 catalyst.

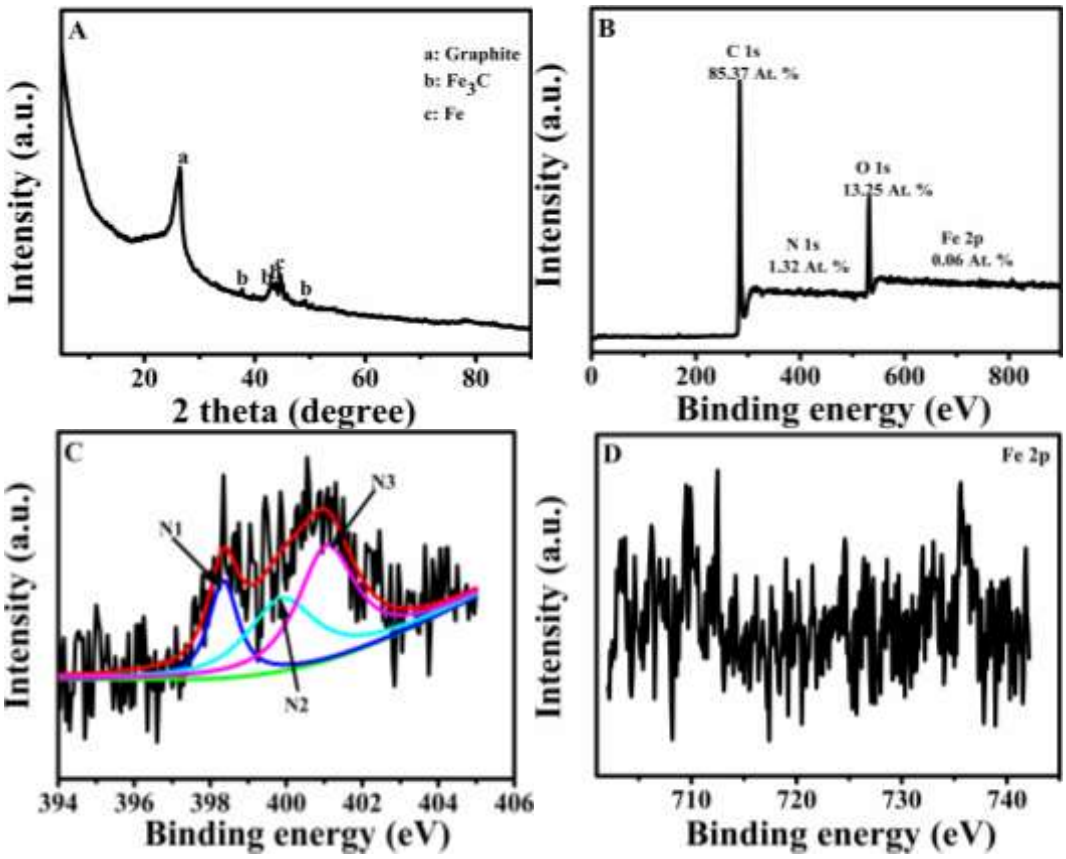

Figure S5 The XRD pattern of NH_2-MIL-101-700 (A); XPS survey spectra (B) of NH_2-MIL-101-700; High resolution N 1s spectra (C) and Fe 2p spectra (D) of the NH_2-MIL-101-700.

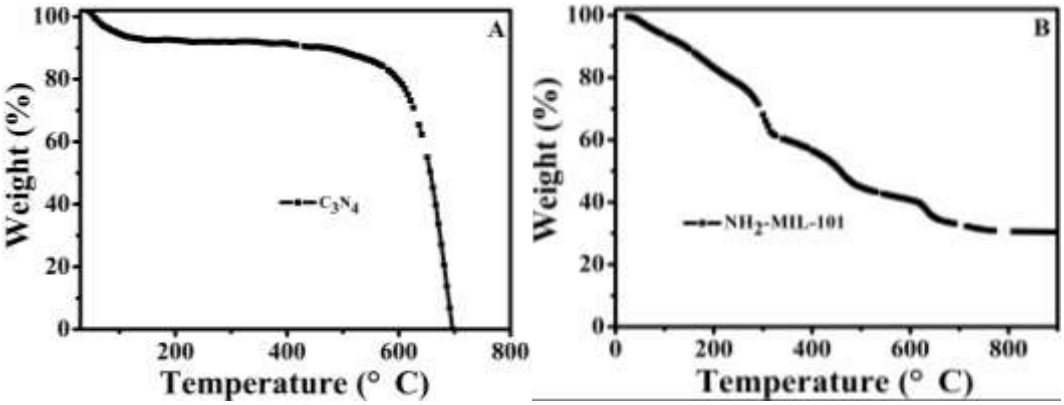

Figure S6 TGA analysis of the C_3N_4(A) and NH_2-MIL-101(B) in N_2 atmosphere.

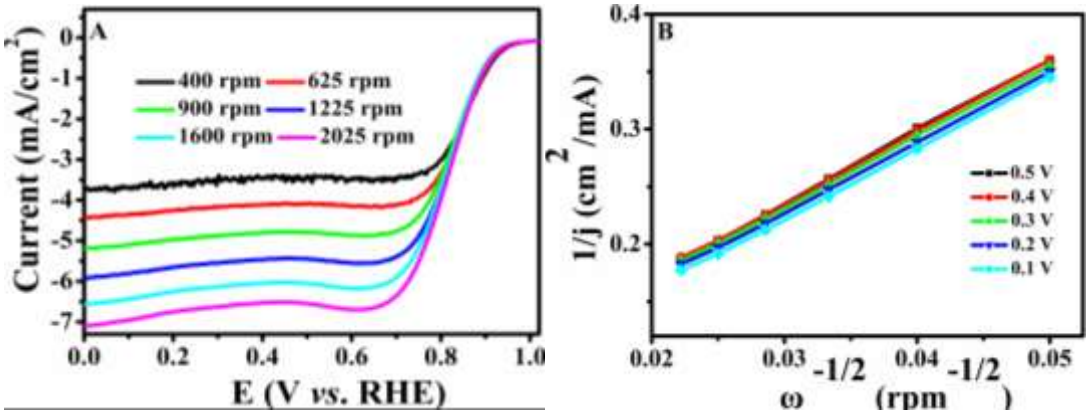

Figure S7 RDE voltammograms (A) of the C_3N_4@NH_2-MIL-101-700 catalyst at various rotation rates in 0.1 M KOH. The corresponding koutecky–levich plots (B) derived from the RDE data.

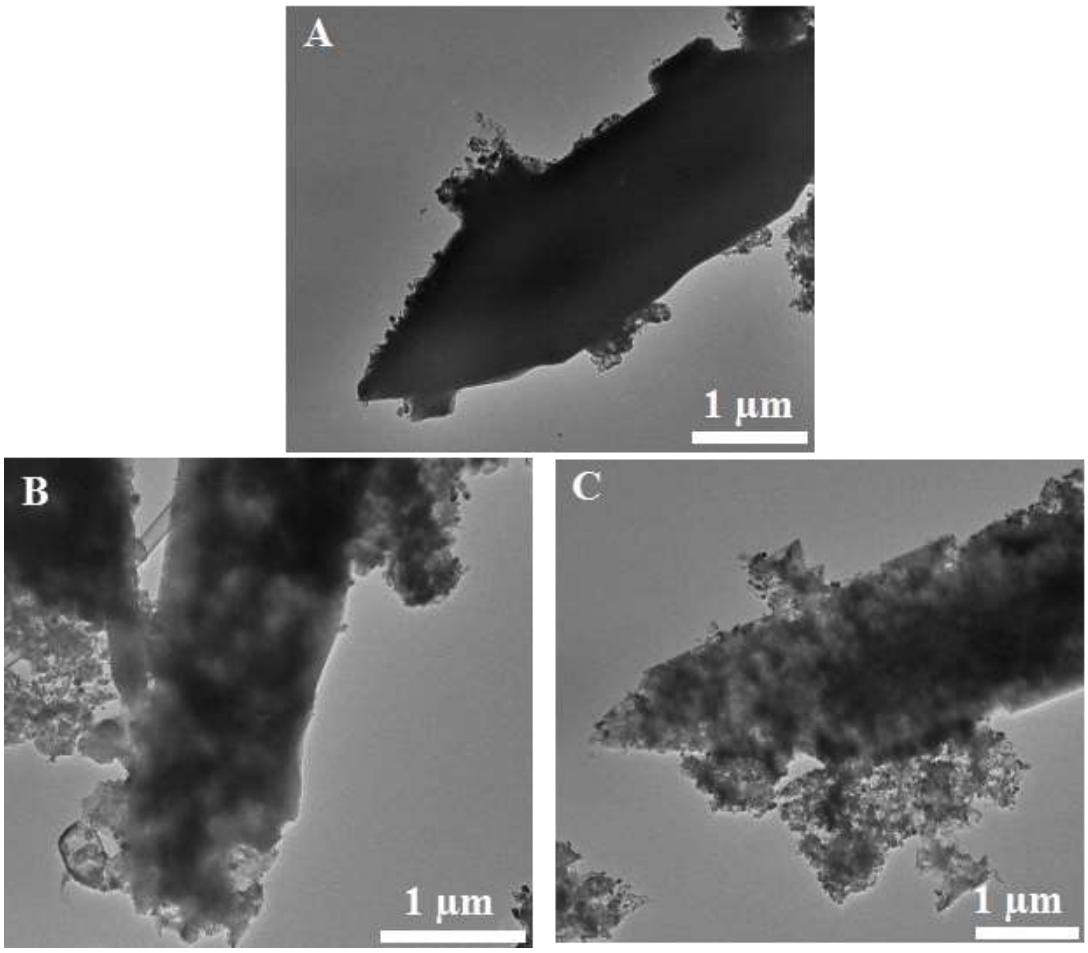

Figure S8 TEM images of the catalysts obtained at different instant pyrolysis temperature, (A) C_3N_4@NH_2-MIL-101-600, (B) C_3N_4@NH_2-MIL-101-800, and (C) C_3N_4@NH_2-MIL-101-900.

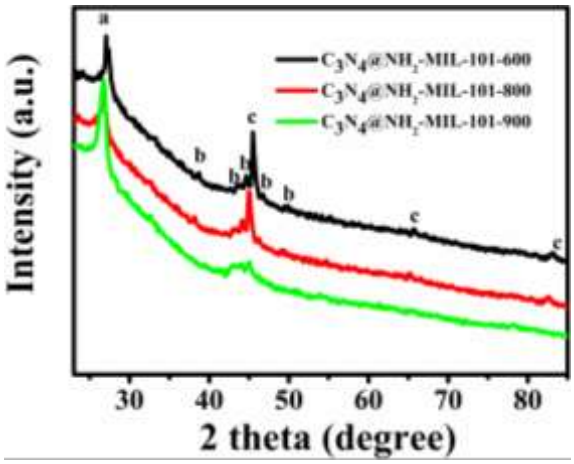

Figure S9 XRD patterns of the catalysts obtained at different pyrolysis temperature.

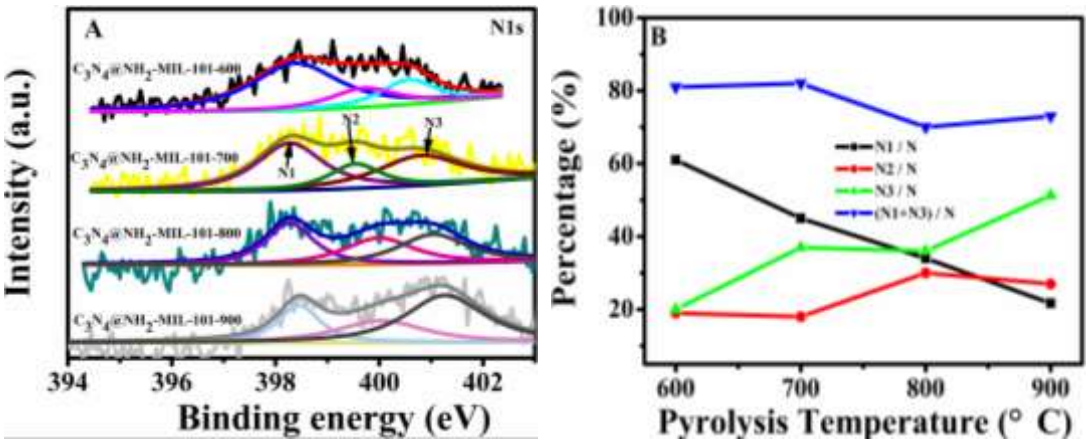

Figure S10 High resolution N 1s spectra (A) of different catalysts. The percentage (B) of various nitrogen as a function of the pyrolysis temperature obtained from the XPS measurements.

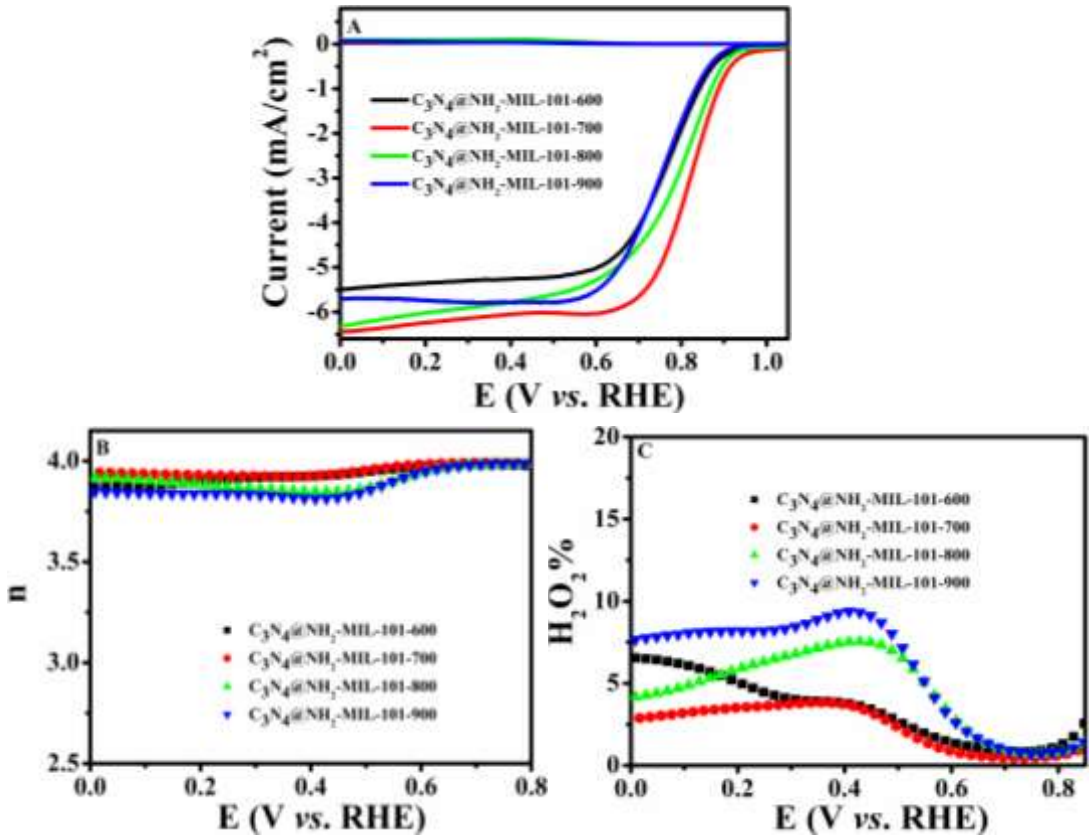

Figure S11 LSV curves (A), electron transfer number (B) and H_2O_2 yield (C) of different catalysts in an O_2-saturated 0.1 M KOH electrolyte with the scan rate of 5 mV/s. Rotation rate is 1600 rpm.

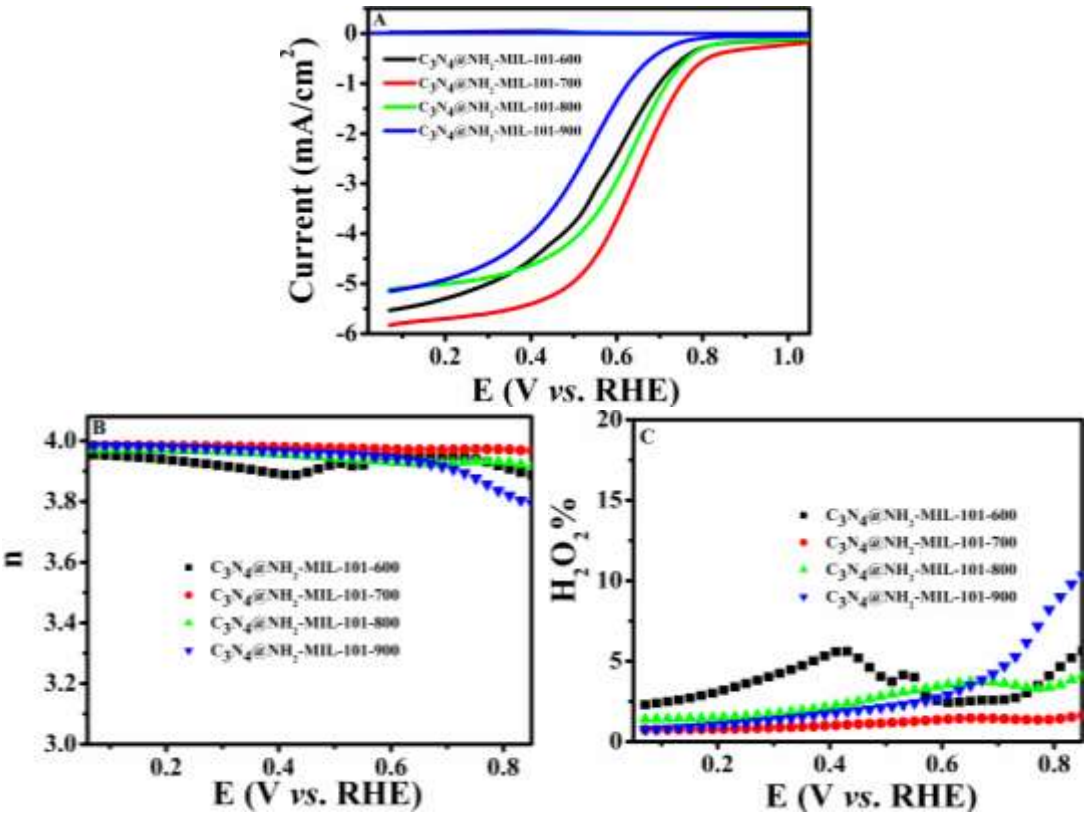

Figure S12 LSV curves (A), electron transfer number (B) and H_2O_2 yield (C) of different catalysts in an O_2-saturated 0.5 M H_2SO_4 electrolyte with the scan rate of 5 mV/s. Rotation rate is 1600 rpm.

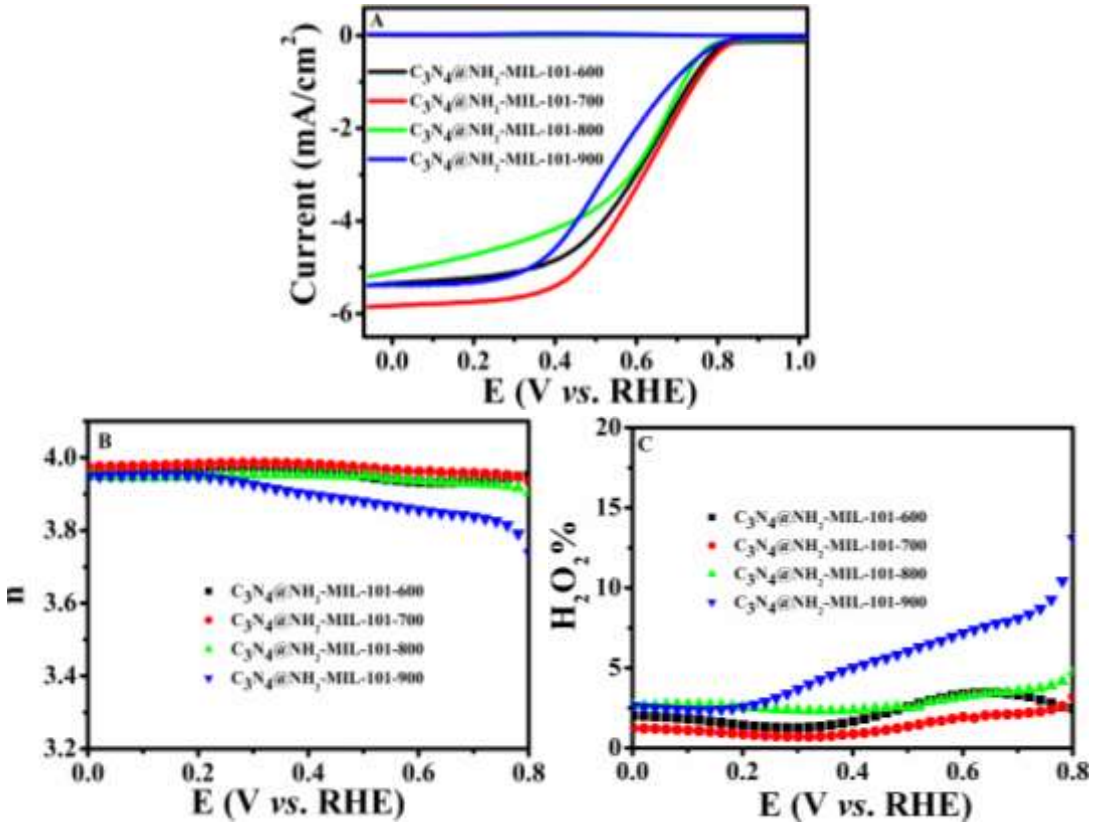

Figure S13 LSV curves (A), electron transfer number (B) and H_2O_2 yield (C) of different catalysts in an O_2-saturated 0.1 M PBS (pH = 7.4) electrolyte with the scan rate of 5 mV/s. Rotation rate is 1600 rpm.

Table S1 The catalyst activity of different catalysts in 0.1 M KOH.

Samples	Electrolyte	Onset potential (V) vs. RHE	Half-wave potential (V) vs. RHE	Current density (mA/cm^2)
NPC-700	0.1 M KOH	0.85	0.68	5.68
NH_2-MIL-101-700	0.1 M KOH	0.90	0.73	5.33
C_3N_4@NH_2-MIL-101-700	0.1 M KOH	0.99	0.84	6.44

Table S2 The catalyst activity of the catalysts at different carbonization temperature.

Samples	onset potential (V) vs. RHE	half-wave potential (V) vs. RHE	current density (mA/cm^2)
C_3N_4@NH_2-MIL-101-600	0.94	0.78	5.5
C_3N_4@NH_2-MIL-101-700	0.99	0.84	6.44
C_3N_4@NH_2-MIL-101-800	0.95	0.80	6.3
C_3N_4@NH_2-MIL-101-900	0.93	0.77	5.7

Table S3 Comparison of the ORR ability of various catalysts.

Catalysts	Electrolyte	E_{onset} (V) vs. RHE	$E_{1/2}$ (V) vs. RHE	Electron transfer number (n)	Reference
C_3N_4@NH_2-MIL-101-700	0.1 M KOH	0.99	0.84	3.94-3.98	This work
	0.5 M H_2SO_4	0.92	0.67	3.97-3.98	
	0.1 M PBS	0.90	0.65	3.94-3.97	
Fe-N/C-800	0.1 M KOH	0.923	0.8	3.9	1
	0.1 M $HClO_4$	0.72	0.55	3.97	
N-doped Fe/Fe_3C@C	0.1 M KOH	0.91	0.83	3.52-3.08	2
LDH@ZIF-67-800	0.1 M KOH	0.94	0.83	3.86-3.98	3
Cu-CTF/CP	0.1 M PBS	0.81	0.59	3.75-3.95	4
Fe-P-C	0.1 M KOH	0.95	—	3.62	5
	0.1 M $HClO_4$	0.84	0.52	3.8	
FeIM/ZIF-8	0.1 M $HClO_4$	0.915	0.755	3.70-3.81	6
P-Z8-Te-1000	0.1 M KOH	0.90	0.80	—	7
NC900 (ZIF-8)	0.1 M KOH	0.83	0.68	3.3	8

—: no data presented.

References

(1) Lin, L.; Zhu, Q.; Xu, A. W. Noble-Metal-Free Fe–N/C Catalyst for Highly Efficient Oxygen Reduction Reaction under Both Alkaline and Acidic Conditions. *J. Am. Chem. Soc.* **2014**, *136*, 11027-11033.

(2) Hou, Y.; Huang, T.; Wen, Z.; Mao, S.; Cui, S.; Chen, J. Metal−Organic Framework-Derived Nitrogen-Doped Core-Shell-Structured Porous Fe/Fe_3C@C Nanoboxes Supported on Graphene Sheets for Efficient Oxygen Reduction Reactions. *Adv. Energy Mater.* **2014**, *4*, 1400337.

(3) Li, Z. H.; Shao, M. F.; Zhou, L.; Zhang, R. K.; Zhang, C.; Wei, M.; Evans, D. G.; Duan, X. Directed Growth of Metal-Organic Frameworks and Their Derived Carbon-Based Network for Efficient Electrocatalytic Oxygen Reduction. *Adv. Mater.* **2016**, *28*, 2337-2344.

(4) Iwase, K.; Yoshioka, T.; Nakanishi, S. J.; Hashimoto, K.; Kamiya, K. Copper-Modified Covalent Triazine Frameworks as Non-Noble-Metal Electrocatalysts for Oxygen Reduction. *Angew. Chem. Int. Ed.* **2015**, *54*, 11068-11072.

(5) Singh, K. P.; Bae, E. J.; Yu, J. S. Fe–P: A New Class of Electroactive Catalyst for Oxygen Reduction Reaction. *J. Am. Chem. Soc.* **2015**, *137*, 3165-3168.

(6) Zhao, D.; Shui, J.; Chen, C.; Chen, X.; Reprogle, B. M.; Wang, D.; Liu, D. Iron Imidazolate Framework as Precursor for Electrocatalysts in Polymer Electrolyte Membranefuel Cells. *Chem. Sci.* **2012**, *3*, 3200-3205.

(7) Zhang, W.; Wu, Z.; Jiang, H.; Yu, S. Nanowire-Directed Templating Synthesis of Metal–Organic Framework Nanofibers and Their Derived Porous Doped Carbon Nanofibers for Enhanced Electrocatalysis *J. Am. Chem. Soc.* **2014**, *136*, 14385-14388.

(8) Aijaz, A.; Fujiwara, N.; Xu, Q. From Metal–Organic Framework to Nitrogen-Decorated Nanoporous Carbons: High CO_2 Uptake and Efficient Catalytic Oxygen Reduction. *J. Am. Chem. Soc.* **2014**, *136*, 6790-6793.